Journal of Iraqi Al-Khwarizmi (JIKh) Volume:10 Issue:2 Year: 2026 pages: 766-776

Evaluating Magnetohydrodynamic and Micropolar Coupling Effects on Blood Flow through an Overlapping Stenosed Artery

Authors Names

Ahmed Bakheet

Publication date: 19/11 /2026
Keywords:Numerical simulation; micropolar fluid; magnetohydrodynamics; overlapping stenosis; stream function–vorticity method.

ABSTRACT

Magnetohydrodynamic (MHD) effects on the steady flow of blood, modelled as a micropolar fluid, through an artery with an axisymmetric overlapping stenosis were investigated. The micropolar model accounts for the micro-rotation of the suspended blood cells through an additional angular momentum equation. The governing equations were mapped onto a rectangular computational domain by a radial coordinate transformation, written in stream function–vorticity–microrotation form, discretized by a finite difference technique with second-order upwinding, and marched in time to the steady state. The solver was validated against the exact fully developed micropolar solution, and grid independence was verified. The effects of the Hartmann number and of the micropolar coupling number on the axial velocity, microrotation, wall shear stress, pressure drop and streamline patterns are presented graphically and in tables. The results show that the magnetic field and the micropolar coupling both raise the wall shear stress and the pressure drop, while both shorten the recirculation zone that forms downstream of the stenosis.

1. Introducation

Stenosis is an abnormal increase in the thickness of the arterial wall that can develop at various locations in the vascular system under diseased conditions [1]. It can form in irregular shapes or as multiple or overlapping stenosis [2, 3]. Chakravarty and Mandal [4] stated that the presence of an overlapping stenosis in the artery is more critical than that of a mild one, and they modelled blood as a Newtonian fluid [4, 5, 6]. The Newtonian model was further used to establish the impact of the overlapping constriction on the flow [7], and many non-Newtonian descriptions of blood were later applied to this geometry, for instance the Sisko model [8], the power-law model [9, 10], the Jeffrey model [11], the Casson model [12, 13, 14], couple stress fluids [15], polar fluids [16] and two-layered models [3, 17–19].

Blood is a suspension of cells in plasma, and the rotation of these cells is not described by classical continuum models. The theory of micropolar fluids, introduced by Eringen [20] (see also [21]), adds an independent microrotation field and an angular momentum balance to the Navier–Stokes equations, and it reduces to the Newtonian model when the coupling (vortex viscosity) vanishes. Haghighi et al. [22] studied micropolar flow through an overlapping stenosis, and Alnussairy and Bakheet [23] considered MHD micropolar flow through a multiple stenosed artery. Recently, Bakheet and Alnussairy [14] simulated the MHD flow of a Casson fluid through an overlapping stenosed artery by the pressure correction method.

In the present paper the Casson model of [14] is replaced by the micropolar model. Blood flow through an overlapping stenosis under a transverse magnetic field is considered, assumed axisymmetric and two-dimensional. The equations are mapped onto a rectangular domain, written in stream function–vorticity–microrotation form and solved by a finite difference method. Compared with [22] and [23], the present work combines the magnetic field and the micropolar coupling in the overlapping geometry, computes the pressure drop across each part of the stenosis, and quantifies the separation and reattachment points of the recirculation zone for a range of both parameters.

Department of Mathematics, College of Science, Mustansiriyah University, Baghdad, Iraq, ahmedbakheet@uomustansiriyah.edu.iq

2. Formation of the Governing Equations

Consider the flow of blood through a straight artery of radius R_0 with an axisymmetric overlapping stenosis, in dimensionless form, as shown in Figure 1 [6]:

$$R(z) = \begin{cases} 1 - \dfrac{3\delta}{2{L_0}^4}[11(z-d){L_0}^3 - 47(z-d)^2{L_0}^2 + 72(z-d)^3L_0 - 36(z-d)^4], & d \le z \le d + L_0 \\ 1, \quad otherwise \end{cases} \quad (1)$$

where $R(z)$ is the radius of the stenosed artery, d indicates the location of the stenosis, L_0 its length and δ a parameter controlling its height. The two throats of the stenosis lie at $z - d \approx 0.188L_0$ and $z - d \approx 0.812L_0$, where $R = 1 - 1.260\delta$.

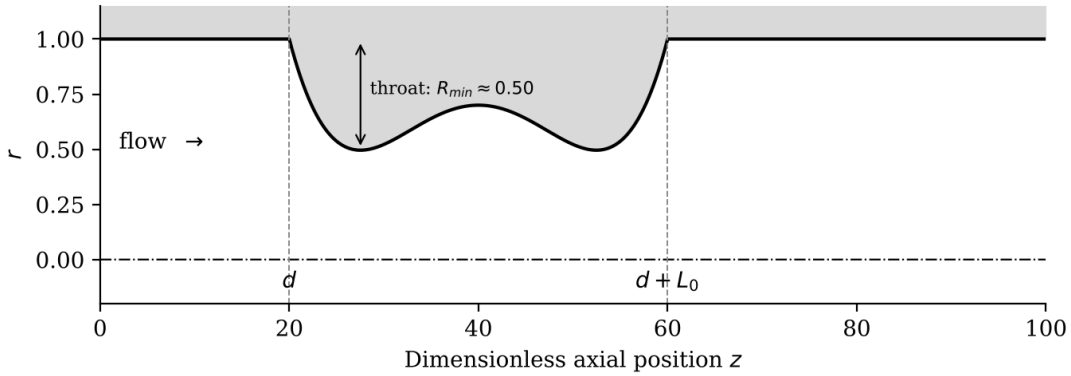


Figure 1- The geometry of the overlapping stenosis (δ = 0.4, d = 20, L₀ = 40).

Blood is treated as an incompressible, electrically conducting micropolar fluid of density ρ, dynamic viscosity μ, vortex viscosity κ, microinertia j and spin-gradient viscosity γ, subject to a uniform transverse magnetic field B_0 (the induced field is neglected). For axisymmetric flow the velocity is $(u, 0, w)$ and the microrotation vector is $(0, c, 0)$. The constitutive equations of the micropolar fluid are [20, 21]

$$t_{ij} = -p\delta_{ij} + \mu(v_{i,j} + v_{j,i}) + \kappa(v_{j,i} - \varepsilon_{ijk}c_k), \quad m_{ij} = \alpha c_{k,k}\delta_{ij} + \beta c_{i,j} + \gamma c_{j,i}, \quad (2)$$

where t_{ij} is the (non-symmetric) stress tensor and m_{ij} the couple stress tensor. Scaling r, z with R_0, u, w with the mean inlet velocity U_0, t with R_0/U_0, p with $\rho{U_0}^2$ and c with U_0/R_0, the governing equations in cylindrical coordinates become

$$\frac{1}{r}\frac{\partial(ru)}{\partial r} + \frac{\partial w}{\partial z} = 0, \quad (3)$$

$$\frac{\partial u}{\partial t} + u\frac{\partial u}{\partial r} + w\frac{\partial u}{\partial z} = -\frac{\partial p}{\partial r} + \frac{1+K}{\mathrm{Re}}\left(\nabla^2 u - \frac{u}{r^2}\right) - \frac{K}{\mathrm{Re}}\frac{\partial c}{\partial z}, \quad (4)$$

$$\frac{\partial w}{\partial t} + u\frac{\partial w}{\partial r} + w\frac{\partial w}{\partial z} = -\frac{\partial p}{\partial z} + \frac{1+K}{\mathrm{Re}}\nabla^2 w + \frac{K}{\mathrm{Re}}\frac{1}{r}\frac{\partial(rc)}{\partial r} - \frac{M^2}{\mathrm{Re}}w, \quad (5)$$

$$j\left(\frac{\partial c}{\partial t} + u\frac{\partial c}{\partial r} + w\frac{\partial c}{\partial z}\right) = \frac{1}{\mathrm{Re}}\left[\bar{\gamma}\left(\nabla^2 c - \frac{c}{r^2}\right) + K\left(\frac{\partial u}{\partial z} - \frac{\partial w}{\partial r}\right) - 2Kc\right] \quad (6)$$

where $\nabla^2 = \frac{\partial^2}{\partial r^2} + \frac{1}{r}\frac{\partial}{\partial r} + \frac{\partial^2}{\partial z^2}$, and the dimensionless parameters are

$$\mathrm{Re} = \frac{\rho U_0 R_0}{\mu}, \qquad K = \frac{\kappa}{\mu}, \qquad \bar{j} = \frac{j}{{R_0}^2}, \qquad \bar{\gamma} = \frac{\gamma}{\mu {R_0}^2}, \qquad M = R_0 B_0 \sqrt{\left(\frac{\sigma}{\mu}\right)} \tag{7}$$

Here Re is the Reynolds number, K the micropolar coupling number, $\bar{j}$ the microinertia, $\bar{\gamma}$ the spin-gradient viscosity parameter, M the Hartmann number and σ the electrical conductivity. Following common practice we take $\gamma = (\mu + \kappa/2)j$, i.e. $\bar{\gamma} = (1 + K/2)\bar{j}$ [21]. For $K = 0$ equations (3)–(5) reduce to the Navier–Stokes equations of a Newtonian fluid with a Lorentz force, and equation (6) decouples.

Boundary conditions. No-slip and no-spin (strict adherence) conditions hold on the arterial wall, and symmetry holds on the axis:

$$u = w = 0, \qquad c = 0 \;\; on \;\; r = R(z); \quad u = 0, \qquad \frac{\partial w}{\partial r} = 0, \qquad c = 0 \;\; on \;\; r = 0. \tag{8}$$

At the inlet $z = 0$ the fully developed MHD micropolar profile $w = w_0(r), c = c_0(r), u = 0$ is prescribed. It is the solution of the two-point boundary value problem

$$(1 + K)\left({w_0}'' + \frac{{w_0}'}{r}\right) + K\left({c_0}' + \frac{c_0}{r}\right) - M^2 w_0 = G, \;\; \bar{\gamma}\left({c_0}'' + \frac{{c_0}'}{r} - \frac{c_0}{r^2}\right) - K{w_0}' - 2Kc_0 = 0, \tag{9}$$

with ${w_0}'(0) = w_0(1) = c_0(0) = c_0(1) = 0$, where the constant pressure gradient G is fixed by the unit mean velocity condition $2\int_0^1 w_0 r \, dr = 1$. For $M = 0$ the problem has the closed-form solution

$$c_0 = \frac{G}{2(2+K)}\left[\frac{I_1(mr)}{I_1(m)} - r\right], \;\; w_0 = \frac{1}{1+K}\left[\frac{G(r^2-1)}{4} - \frac{KG}{2(2+K)}\left(\frac{I_0(mr) - I_0(m)}{mI_1(m)} - \frac{r^2-1}{2}\right)\right] \tag{10}$$

with $m^2 = \frac{K(2+K)}{\bar{\gamma}(1+K)}$, where I_0 and I_1 are modified Bessel functions; it is used below to validate the solver. At the outlet $z = L$ all quantities satisfy $\partial/\partial z = 0$.

3. Solution Development

Introducing the stream function ψ and the vorticity Ω by

$$u = -\frac{1}{r}\frac{\partial \psi}{\partial z}, \;\; w = \frac{1}{r}\frac{\partial \psi}{\partial r}, \;\; \Omega = \frac{\partial u}{\partial z} - \frac{\partial w}{\partial r}, \tag{11}$$

the continuity equation (3) is satisfied identically, and eliminating the pressure from (4)–(5) gives

$$E^2\psi \equiv \frac{\partial^2 \psi}{\partial r^2} - \frac{1}{r}\frac{\partial \psi}{\partial r} + \frac{\partial^2 \psi}{\partial z^2} = -r\Omega, \tag{12}$$

$$\frac{\partial \Omega}{\partial t} + u\frac{\partial \Omega}{\partial r} + w\frac{\partial \Omega}{\partial z} - \frac{u\Omega}{r} = \frac{1+K}{\mathrm{Re}}\left(\nabla^2\Omega - \frac{\Omega}{r^2}\right) - \frac{K}{\mathrm{Re}}\left(\nabla^2 c - \frac{c}{r^2}\right) + \frac{M^2}{\mathrm{Re}}\frac{\partial w}{\partial r}, \tag{13}$$

together with the microrotation equation (6), in which $\frac{\partial u}{\partial z} - \frac{\partial w}{\partial r} = \Omega$. To map the constricted domain into a rectangular one and avoid interpolation at the curved wall, the transformation $\xi = r/R(z)$ is adopted [14], so that $0 \le \xi \le 1$. The derivatives transform as

$$\frac{\partial}{\partial r} = \frac{1}{R}\frac{\partial}{\partial \xi}, \qquad \left(\frac{\partial}{\partial z}\right)_r = \frac{\partial}{\partial z} - a\frac{\partial}{\partial \xi}, \qquad \frac{\partial^2}{\partial r^2} = \frac{1}{R^2}\frac{\partial^2}{\partial \xi^2}, \tag{14}$$

$$\left(\frac{\partial^2}{\partial z^2}\right)_r = \frac{\partial^2}{\partial z^2} - 2a\frac{\partial^2}{\partial z \partial \xi} + a^2\frac{\partial^2}{\partial \xi^2} + b\frac{\partial}{\partial \xi}, \quad a = \frac{\xi R'}{R}, \qquad b = \xi\left(\frac{2R'^2}{R^2} - \frac{R''}{R}\right) \tag{15}$$

Applying (14)–(15) to (12), (13) and (6) gives the transformed equations on the rectangle $0 \le \xi \le 1, 0 \le z \le L$. The boundary conditions become $\psi = 0, \Omega = 0, c = 0$ on $\xi = 0$; $\psi = \psi_w, c = 0$ on $\xi = 1$, where $\psi_w = \int_0^1 r w_0 dr = \frac{1}{2}$ is the volume flux; the inlet values of ψ, Ω, c follow from the inlet profile, and $\partial/\partial z = 0$ at $z = L$. On the wall ψ is constant and $\partial\psi/\partial\xi = 0$ (no slip), so (12) yields the wall vorticity

$$\Omega_w = -\frac{1 + R'^2}{R^3}\left(\frac{\partial^2 \psi}{\partial \xi^2}\right)_{\xi=1} \approx -\frac{1 + R'^2}{R^3}\frac{8\psi_{N-1} - \psi_{N-2} - 7\psi_w}{2\Delta\xi^2} \tag{16}$$

which is the second-order formula of Briley [24] (a refinement of Thom's formula [25]). Because $c = 0$ on the wall, the micropolar shear stress on the wall reduces to $(\mu + \kappa)\partial v_t/\partial n$, which in dimensionless form (scaled by $\mu U_0/R_0$) is

$$\tau_w = (1 + K)\Omega_w. \tag{17}$$

Positive τ_w corresponds to forward flow at the wall and negative values indicate flow separation. The pressure is recovered by integrating the steady axial momentum equation (5) along the axis, where $u = 0$ and, since $\nabla^2 v = -\nabla \times (\Omega e\theta)$,

$$\left(\frac{\partial p}{\partial z}\right)_{r=0} = -w\frac{\partial w}{\partial z} - \frac{2(1 + K)}{\mathrm{Re}}\frac{\partial \Omega}{\partial r} + \frac{2K}{\mathrm{Re}}\frac{\partial c}{\partial r} - \frac{M^2}{\mathrm{Re}}w. \tag{18}$$

4. Numerical Procedure

The transformed equations were discretized on a uniform grid $\xi_j = j\Delta\xi, z_i = i\Delta z$ with $\Delta\xi = 1/40$ and $\Delta z = 0.2$ (41 × 501 nodes for $L = 100$). Diffusion and metric terms, including the mixed derivative $\partial^2/\partial z \partial \xi$, were approximated by second-order central differences, and the convective terms by second-order upwind differences written in terms of the contravariant velocities $W = w$ and $V = u/R - aw$. The vorticity and microrotation equations were advanced by explicit time stepping with $\Delta t = 0.003$, and after each step the elliptic equation (12) for ψ was solved by a direct sparse LU factorization, computed only once since the transformed operator does not change in time. The wall vorticity (16) was then updated with under-relaxation factor 0.5. The computation was started from the inlet profile and stopped when $max|\partial\Omega/\partial t|$ and $max|\partial c/\partial t|$ fell below 2×10^{-5}, which defines the steady state.

Validation.

For $\delta = 0$ (straight tube) the steady solution must reproduce the fully developed solution (10). Figure 2 compares the computed axial velocity and microrotation at $z = 25$ with the exact solution for $K = 0, 0.5, 2$ (Re = 300); the maximum differences are below 1.6×10^{-3} for w and 3.7×10^{-3} for c. For $K = 0$ the computed wall shear stress is 3.999 against the Poiseuille value 4, and the axial pressure gradient from (18) agrees with G/Re of the boundary value problem to within 0.05% for $K = 0$, $K = 1$ and $K = 1, M = 4$.

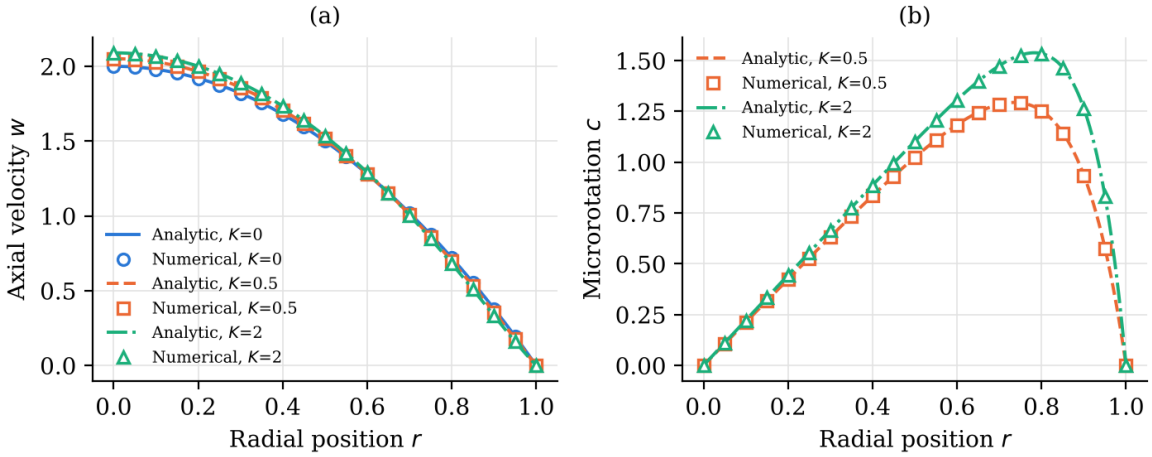


Figure 2- Comparison of the numerical and exact fully developed solutions in a straight tube: (a) axial velocity, (b) microrotation.

Grid independence. Table 1 compares the results of the working grid with a refined grid ($\Delta\xi = 1/60, \Delta z = 0.1, \Delta t = 0.0012$) for $M = 0, K = 0.5$. All quantities differ by less than 3%, and most by less than 0.3%; the working grid was therefore used for all computations.

Table 1- Grid independence test (M = 0, K = 0.5)

Quantity	**41 × 501 grid**	**61 × 1001 grid**	**Difference (%)**
Pressure drop across first stenosis	13.987	13.986	0.00
Pressure drop across second stenosis	9.729	9.456	2.81
Pressure drop across the artery	22.476	22.303	0.77
Peak wall shear stress, first throat	87.642	87.626	0.02
Peak wall shear stress, second throat	71.357	71.374	0.02
Separation point	57.000	56.900	0.18
Reattachment point	86.800	86.600	0.23

5. Numerical Results and Discussion

The results are presented for $\mathrm{Re} = 300, d = 20, L_0 = 40, \delta = 0.4, L = 100, \bar{j} = 0.01$, with $M = 0, 4, 8$ and $K = 0$ (Newtonian), 0.5, 1, 2. With $\delta = 0.4$ the radius at both throats is $R \approx 0.50$ (75% area reduction). Unless stated otherwise $K = 0.5$ when M varies and $M = 0$ when K varies.

Figure 3 shows the axial velocity at five axial stations. The flow accelerates strongly through the throats, where the centreline velocity rises from about 2 upstream to 5.75 at the first throat and 6.68 at the second throat; the profiles become blunt there because of the thin boundary layers at $\mathrm{Re} = 300$. Between the throats ($z = 40$) the flow decelerates, and downstream of the stenosis ($z = 70$) a jet persists in the core while the velocity near the wall becomes negative, indicating backflow.

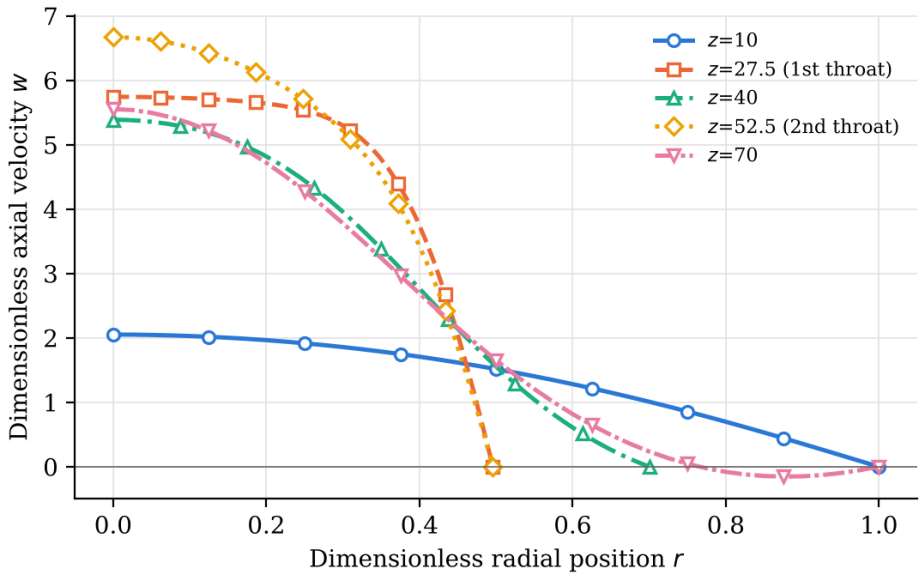


Figure 3- Axial velocity profiles at different axial positions (M = 0, K = 0.5).

Figure 4 displays the influence of the Hartmann number. At the second throat the magnetic field flattens the profile: the centreline velocity decreases from 6.68 ($M = 0$) to 6.37 ($M = 4$) and 5.87 ($M = 8$) while the velocity near the wall increases, because the Lorentz force acts against the fastest fluid. The effect is much stronger downstream ($z = 70$), where the centreline velocity drops from 5.55 to 4.59 and 2.39, and the negative near-wall velocity disappears as M increases, so the magnetic field helps to prevent backflow.

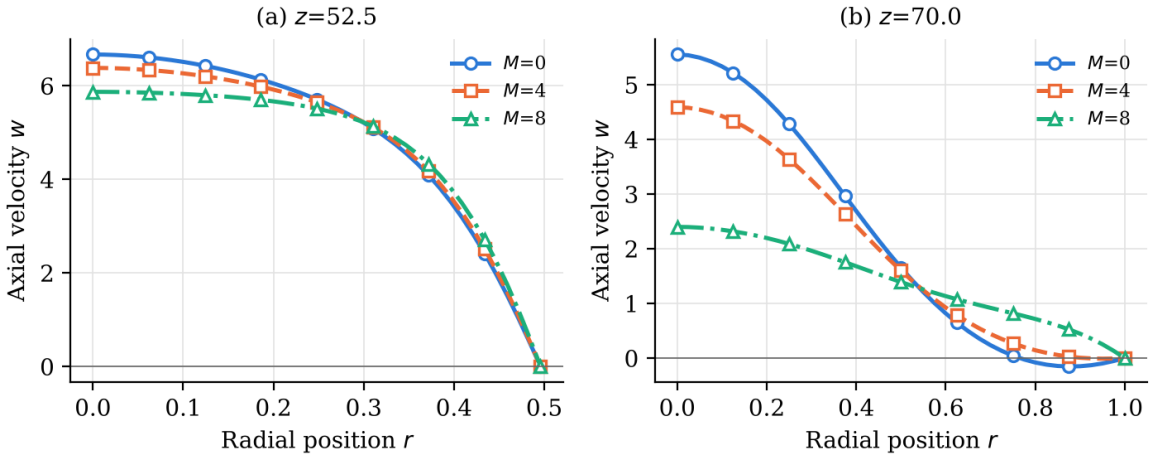


Figure 4- Effect of the Hartmann number on the axial velocity (K = 0.5): (a) second throat, (b) downstream of the stenosis.

Figure 5 shows the effect of the coupling number K. Increasing K increases the effective resistance near the wall, which pushes the flow towards the axis: at the second throat the centreline velocity increases from 6.43 (Newtonian) to 7.05 for $K = 2$, with lower velocities close to the wall. Downstream the profiles are less sensitive to K, but the region of reversed flow becomes weaker.

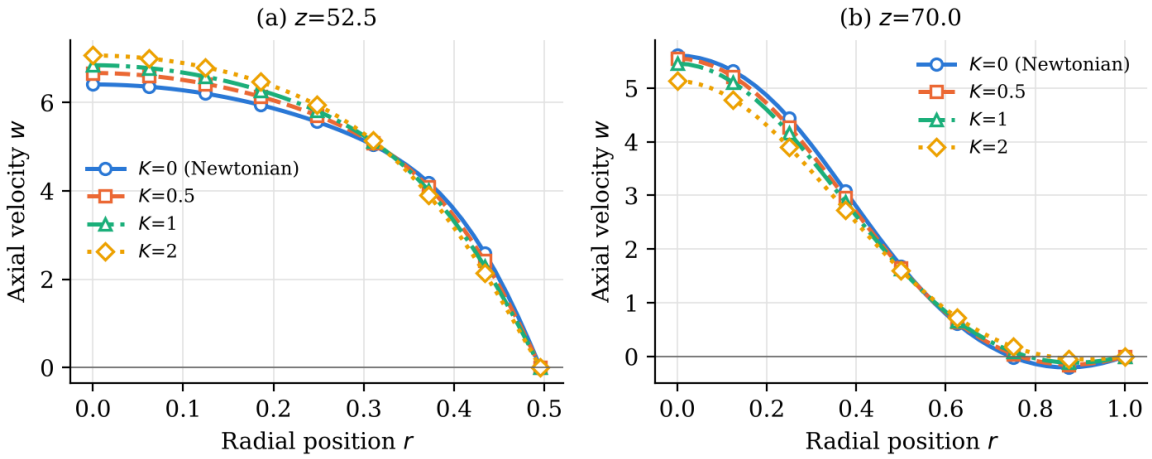


Figure 5- Effect of the coupling number on the axial velocity (M = 0): (a) second throat, (b) downstream of the stenosis.

The microrotation at the second throat is shown in Figure 6. It vanishes on the axis and on the wall and reaches a maximum close to the wall, where the velocity gradient is largest; it is positive, in the same sense as the vorticity of the flow. The magnetic field reduces the microrotation in the core, in line with the flatter velocity profile, while increasing K increases it considerably (the maximum grows from about 4.5 for $K = 0.5$ to 7.9 for $K = 2$), because K is the coupling between the vorticity and the microrotation in equation (6).

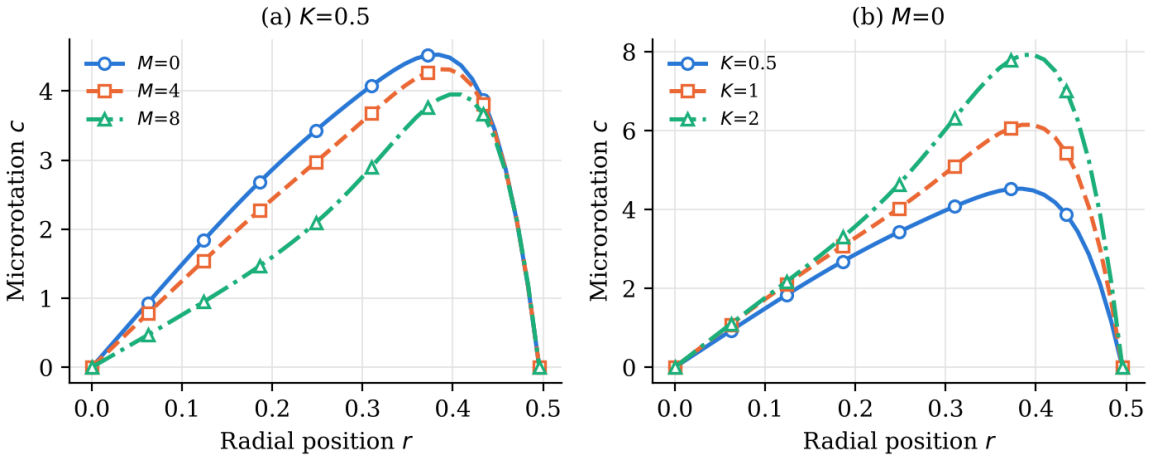


Figure 6- Microrotation profiles at the second throat: (a) effect of M (K = 0.5), (b) effect of K (M = 0).

Figure 7 reveals that the wall shear stress increases sharply to reach its maximum at the two throats, with the larger peak at the first throat (87.64 against 71.36 for $M = 0, K = 0.5$). It then falls to negative values just downstream of the stenosis, which marks the separation of the flow. Increasing M increases the wall shear stress everywhere (the first peak becomes 90.10 and 96.34 for $M = 4$ and 8) and shrinks the region of negative shear stress. Increasing K raises the wall shear stress even more (first peak 67.82, 87.64, 104.69 and 134.43 for $K = 0, 0.5, 1, 2$), since the wall stress is multiplied by $(1 + K)$ in (17).

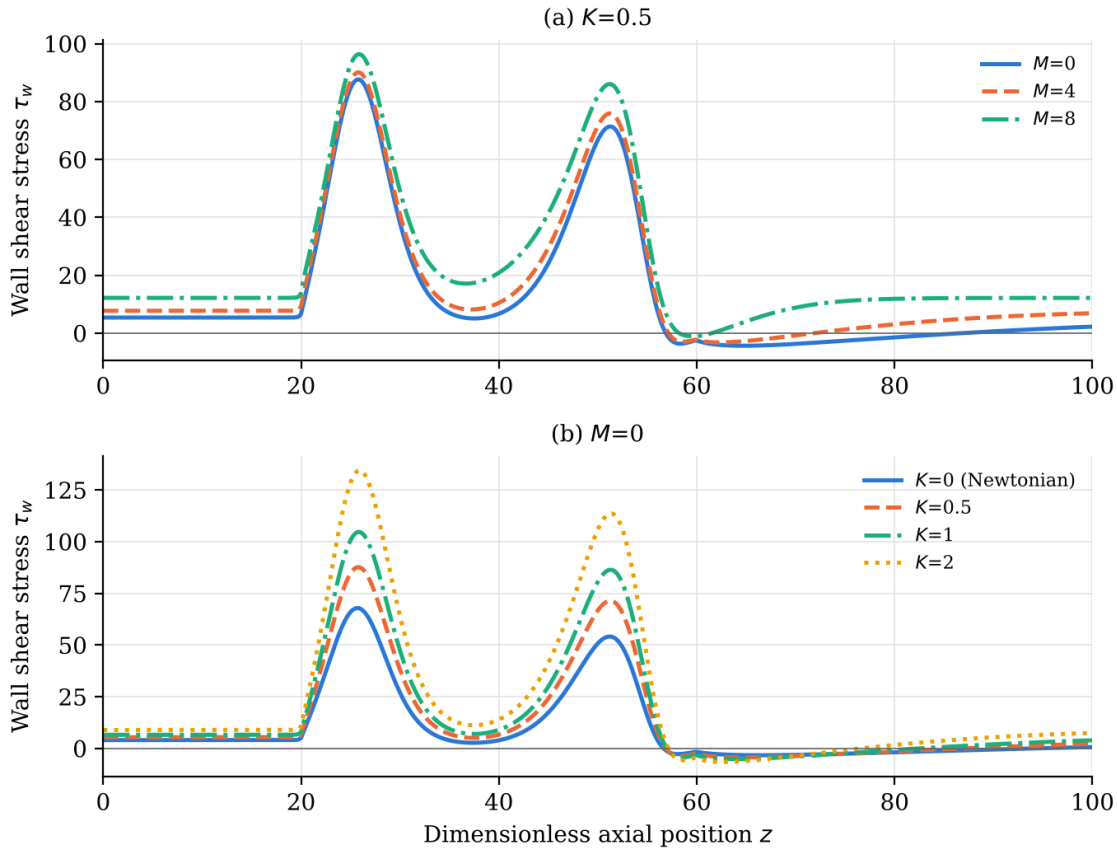


Figure 7- Variation of the wall shear stress with axial distance: (a) different M (K = 0.5), (b) different K (M = 0).

Table 2 gives the dimensionless pressure drop along the axis across the first stenosis ($20 \leq z \leq 40$), the second stenosis ($40 \leq z \leq 60$) and the whole artery for different values of M. The pressure drop increases considerably with the magnetic intensity: across the artery it rises from 22.48 to 33.63 and 66.06. The drop across the second stenosis is larger than across the first.

Table 2- Dimensionless pressure drop across the overlapping stenosis (K = 0.5)

	M = 0	**M = 4**	**M = 8**
Pressure drop across first stenosis	9.73	13.47	23.87
Pressure drop across second stenosis	13.99	17.09	26.49
Pressure drop across the artery	22.48	33.63	66.06

Table 3 combines both parameters. For every value of M the pressure drop across the artery increases with K (for $M = 0$ from 18.40 for Newtonian blood to 33.14 for $K = 2$), so neglecting the micropolar character of blood underestimates the pressure drop. The table also lists the separation and reattachment points of the recirculation zone (where τ_w changes sign). The separation point stays close to the end of the stenosis, but the reattachment point moves upstream when either M or K increases.

Table 3- Pressure drop across the artery and extent of the recirculation zone

K	**M**	**Pressure drop (artery)**	**Separation z**	**Reattachment z**	**Length**
0	0	18.40	56.8	94.2	37.4

(Newtonian)					
	4	28.88	57.0	73.2	16.2
	8	60.23	58.2	61.4	3.2
0.5	0	22.48	57.0	86.8	29.8
	4	33.63	57.2	71.8	14.6
	8	66.06	58.4	61.4	3.0
1	0	26.15	57.0	82.4	25.4
	4	37.73	57.4	70.8	13.4
	8	70.93	58.4	61.4	3.0
2	0	33.14	57.2	76.6	19.4
	4	45.19	57.4	69.0	11.6
	8	79.43	58.4	61.4	3.0

Figure 8 demonstrates the streamline patterns for different values of the Hartmann number. A large recirculation zone develops downstream of the stenosis for $M = 0$ (from $z \approx 57.0$ to $z \approx 86.8$). It shrinks markedly for $M = 4$ ($z \approx 57.2$ to 71.8) and becomes a very small eddy attached to the end of the stenosis for $M = 8$ ($z \approx 58.4$ to 61.4), so the magnetic field almost suppresses the recirculation.

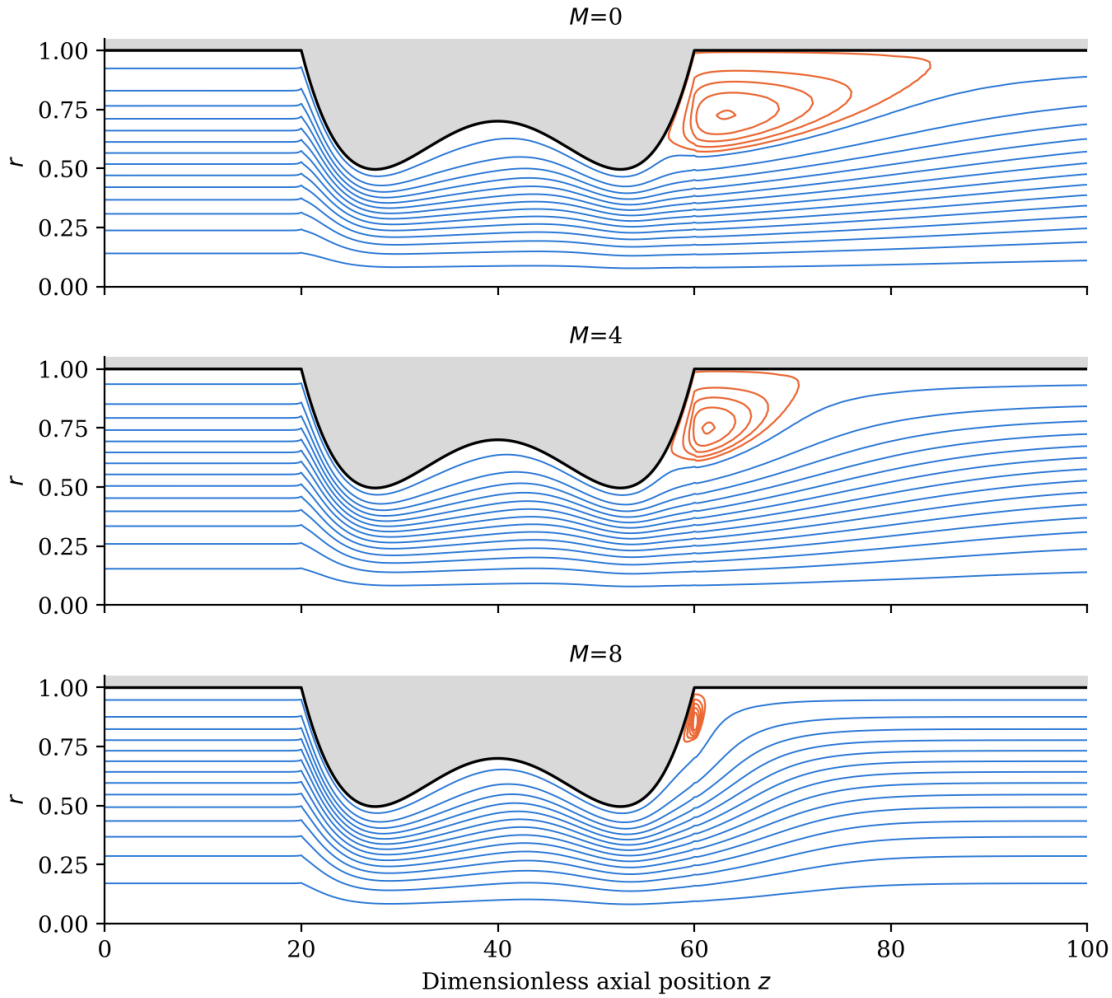


Figure 8- Streamline patterns for different values of M (K = 0.5); recirculating streamlines are drawn in orange.

6. Conclusions

Blood flow through an arterial segment with an overlapping stenosis under a transverse magnetic field was studied with the micropolar model, which accounts for the rotation of the blood cells. The equations were solved in stream function–vorticity–microrotation form on a transformed rectangular domain, and the solver was validated against the exact fully developed solution and by a grid-refinement test. The main findings are:

- The magnetic field flattens the velocity profile at the throats, decelerates the core flow downstream and removes the near-wall backflow;
- The wall shear stress peaks at the throats, with the larger peak at the first throat, and increases with both the Hartmann number and the coupling number;
- The pressure drop increases with the Hartmann number and with the coupling number; the Newtonian model (K = 0) gives the lowest pressure drop;
- The microrotation vanishes on the axis and on the wall, peaks near the wall, decreases with M and increases strongly with K;
- The recirculation zone downstream of the stenosis shortens as M or K increases, and is reduced to a very small eddy for M = 8.

References

1. Onitilo, S., Usman, M. and Daniel, D. 2020. Effects of Hematocrit on Blood Flow through a Stenosed Human Carotid Artery. Iraqi Journal of Science, 2106-2114.
2. Joshi, P., Pathak, A. and Joshi, B.K. 2009. Two layered model of blood flow through composite stenosed artery, Applications and Applied Mathematics. 4(2): 343-354.
3. Srivastava, V. P. and Rastogi, R. 2010. Blood flow through stenosed catheterized artery: effects of hematocrit and stenosis shape, Computers & Mathematics with Applications, 59: 1377-1785.
4. Chakravarty, S. and Mandal, P. K. 1996. A nonlinear two-dimensional model of blood flow in an overlapping arterial stenosis subjected to body acceleration, Mathematical and Computer Modelling, 24: 43–58.
5. Chakravarty, S. and Mandal, P.K. 2000. Two-dimensional blood flow through tapered arteries under stenotic conditions, International Journal of Non-Linear Mechanics, 35: 779–793.
6. Chakravarty, S. and Mandal, P. K. 1994. Mathematical modelling of blood flow through an overlapping arterial stenosis. Mathematical and Computer Modelling, 19: 59-70.
7. Layek, G. Mukhopadhyay, C. S. and Gorla, R. S. D. 2009. Unsteady viscous flow with variable viscosity in a vascular tube with an overlapping constriction, International Journal of Engineering Science, 47: 649-659.
8. Mekheimer, K. S. and El Kot, M. A. 2012. Mathematical modelling of unsteady flow of a Sisko fluid through an anisotropically tapered elastic arteries with time-variant overlapping stenosis, Applied Mathematical Modelling, 36(11): 5393-5407.
9. Ismail, Z., Abdullah, I., Mustapha, N. and Amin, N. 2008. A power-law model of blood flow through a tapered overlapping stenosed artery, Applied Mathematics and Computation, 195(2): 669-680.
10. Zaman, A., Ali, N. and Sajid, M. 2016. Slip effects on unsteady non-Newtonian blood flow through an inclined catheterized overlapping stenotic artery, AIP Advances, 6(1): 015118.
11. Vijaya, R. B. 2017. A mathematical model on Jeffrey fluid flow through an overlapping stenosis, International Journal of Innovative Research in Science, Engineering and Technology, 6(13): 181-186.
12. Srivastava, V. P. Mishra, S. and Rastogi, R. 2010. Non-Newtonian arterial blood flow through an overlapping stenosis, Applications and Applied Mathematics, 5(1): 225-238.

13. Arunkumar, M. 2015. Casson flow of blood through an arterial tube with overlapping stenosis, IOSR J. Math., 11(6): 26-30.
14. Bakheet, A. and Alnussairy, E. A. 2021. Numerical Simulation of Magnetohydrodynamic Influences on Casson Model for Blood Flow through an Overlapping Stenosed Artery. Iraqi Journal of Science, 62(3): 1016-1024. doi: 10.24996/ijs.2021.62.3.30.
15. Prasad, K. M. Thulluri, S. and Phanikumari, M. V. 2017. Investigation of blood flow through an artery in the presence of overlapping stenosis, Journal of Naval Architecture and Marine Engineering, 14(1): 39-46.
16. Reddy, J. V. R. and Srikanth, D. 2015. The polar fluid model for blood flow through a tapered artery with overlapping stenosis: effects of catheter and velocity slip, Applied Bionics and Biomechanics, 2015: 1-13.
17. Srivastava, V. P., Rastogi, R. and Vishnoi, R. 2010. A two-layered suspension blood flow through an overlapping stenosis, Computers & Mathematics with Applications, 60(3): 432-441.
18. Srivastava, V. P., Vishnoi, R., Mishra, S. and Sinha, P. 2011. A two-layered non-Newtonian arterial blood flow through an overlapping constriction, AAM: Int. J., 6(1): 41-57.
19. Srivastava, V. P., Vishnoi, R., Singh, D. and Mishra, S. 2015. Response to blood flow through an overlapping stenosis in catheterized arteries, e-Journal of Science & Technology, 5: 93-103.
20. Eringen, A. C. 1966. Theory of micropolar fluids. Journal of Mathematics and Mechanics, 16(1): 1-18.
21. Łukaszewicz, G. 1999. Micropolar Fluids: Theory and Applications. Birkhäuser, Boston.
22. Haghighi, A. R., Asl, M. S. and Kiyasatfar, M. 2015. Mathematical modeling of micropolar fluid flow through an overlapping arterial stenosis, International Journal of Biomathematics, 8(04): 1550056.
23. Alnussairy, E. A. and Bakheet, A. 2019. MHD Micropolar blood flow model through a multiple stenosed artery. AIP Conference Proceedings, 2183(1): 090002.
24. Briley, W. R. 1971. A numerical study of laminar separation bubbles using the Navier–Stokes equations. Journal of Fluid Mechanics, 47(4): 713-736.
25. Thom, A. 1933. The flow past circular cylinders at low speeds. Proceedings of the Royal Society of London A, 141: 651-669.